BNL-212407-2019-JAAM

Single-atom cobalt array bound to distorted 1T MoS2 with ensemble effect for hydrogen evolution catalysis

K. Qi, P. Liu

To be published in "NATURE COMMUNICATIONS"

October 2019

Chemistry Department

Brookhaven National Laboratory

U.S. Department of Energy

USDOE Office of Science (SC), Basic Energy Sciences (BES) (SC-22)

Notice: This manuscript has been authored by employees of Brookhaven Science Associates, LLC under Contract No. DE-SC0012704 with the U.S. Department of Energy. The publisher by accepting the manuscript for publication acknowledges that the United States Government retains a non-exclusive, paid-up, irrevocable, world-wide license to publish or reproduce the published form of this manuscript, or allow others to do so, for United States Government purposes.

DISCLAIMER

This report was prepared as an account of work sponsored by an agency of the United States Government. Neither the United States Government nor any agency thereof, nor any of their employees, nor any of their contractors, subcontractors, or their employees, makes any warranty, express or implied, or assumes any legal liability or responsibility for the accuracy, completeness, or any third party's use or the results of such use of any information, apparatus, product, or process disclosed, or represents that its use would not infringe privately owned rights. Reference herein to any specific commercial product, process, or service by trade name, trademark, manufacturer, or otherwise, does not necessarily constitute or imply its endorsement, recommendation, or favoring by the United States Government or any agency thereof or its contractors or subcontractors. The views and opinions of authors expressed herein do not necessarily state or reflect those of the United States Government or any agency thereof.

Single-Atom Cobalt Array Bound to Distorted 1T-MoS_2 with Ensemble Effect for Hydrogen Evolution Catalysis

Kun Qi[1], Xiaoqiang Cui[1*], Lin Gu[2], Shansheng Yu[1], Xiaofeng Fan[1], Mingchuan Luo[3,4], Shan Xu[1], Ningbo Li[1], Lirong Zheng[5], Qinghua Zhang[2], Jingyuan Ma[6], Yue Gong[2], Fan Lv[3,4], Kai Wang[3,4], Haihua Huang[1], Wei Zhang[1], Shaojun Guo[3,4*], Weitao Zheng[1*] and Ping Liu[7]

[1] *State Key Laboratory of Automotive Simulation and Control, Department of Materials Science, Key Laboratory of Automobile Materials of MOE, Jilin University, Changchun, 130012, China.*

[2]*Key Laboratory for Renewable Energy, Beijing Key Laboratory for New Energy Materials and Devices, Laboratory of Advanced Materials and Electron Microscopy, Beijing National Laboratory for Condensed Matter Physics, Institute of Physics, Chinese Academy of Sciences, Beijing 100190, China.*

[3]*Department of Materials Science and Engineering, and* [4]*BIC-ESAT, College of Engineering, Peking University, Beijing 100871, China.*

[5]*Beijing Synchrotron Radiation Facility, Institute of High Energy Physics, Chinese Academy of Sciences, Beijing 100049, China.*

[6] *Shanghai Synchrotron Radiation Facility, Shanghai Institute of Applied Physics, Chinese Academy of Sciences, Shanghai 200120, China.*

[7] *Department of Chemistry, Brookhaven National Laboratory, Upton, New York 11973, USA.*

Email: xqcui@jlu.edu.cn (X. Q. Cui); guosj@pku.edu.cn (S. J. Guo); wtzheng@jlu.edu.cn (W. T. Zheng)

The grand challenge in the development of atomically dispersed metallic catalysts is their low metal-atom loading density, uncontrollable localization and ambiguous interactions with supports, posing difficulty in maximizing their catalytic performance. Herein, we achieve a new interface catalyst consisting of single cobalt atom array covalently bound to distorted 1T MoS_2 nanosheets (SA Co-D 1T MoS_2) with ensemble effect for boosting hydrogen evolution reaction (HER) through a new assembly/leaching strategy. The phase transformation of MoS_2 from 2H to D-1T, induced by the strain from lattice mismatch and the formation of Co-S covalent bond between Co and MoS_2 during the assembly of Co nanodisks on MoS_2 nanosheets, is found to be essential to form the highly active single-atom array catalyst. SA Co-D 1T MoS_2 achieves unprecedented Pt-like catalytic behaviour toward the HER and high long-term stability in acid electrolyte. It represents the best HER performance among the reported non-noble-metal catalysts in acid electrolyte. The combined data from an active-site blocking experiment together with density functional theory (DFT) calculations reveal that the superior behaviour of SA Co-D 1T MoS_2 is associated with an ensemble effect *via* the synergy of Co adatom and S of the D-1T MoS_2 support by tuning hydrogen binding mode at the interface.

Hydrogen (H_2), as a zero-emission, renewable energy source, has attracted increasingly extensive attention due to its important role in solving the environmental issues.[1,2] Water splitting catalysis is one of the most efficient approaches for H_2 generation because of its high-efficiency energy conversion.[3] Platinum (Pt) is the best catalyst for the hydrogen evolution reaction (HER); however, the high cost and limited earth abundance of Pt expose tremendous limitations for large-scale implementation.[4] Therefore, the critical determinant for energy storage in electrolytic systems is the development of robust and efficient alternative catalysts that are cheap and earth-abundant. Remarkable advances have been made in developing efficient non-noble materials as Pt substitutes for HER.[5] Unfortunately, a large gap in their HER catalytic performance still exists for completely substituting Pt due to their lack of more efficient active sites and difficulty in maximizing the intrinsic activity of their active sites.[6,7] Atomically dispersed catalysts with single metal atoms or mononuclear metal complexes anchored on supports represent the lowest size limit to achieve maximum atom efficiency, providing the most ideal platform for catalysis.[8-10] However, the biggest issue is that previously reported atomically dispersed catalysts have been primarily in the form of atomic clusters, especially at high loading amounts, due to the ambiguous interactions between the metal atoms and supports, posing a difficulty in maximizing the catalytic efficiency.[11-15]

Herein, we report a new procedure for making single-atom cobalt (Co) array covalently bound onto distorted 1T MoS_2 nanosheets (denoted as SA Co-D 1T MoS_2) *via* Co-S bonds through electrochemical cyclic voltammetry (CV) leaching of Co nanodisks (NDs)-MoS_2 nanosheet hybrids. The strain induced by lattice mismatch and the formation of Co-S covalent bond between Co and MoS_2 in the Co ND-MoS_2 nanosheet hybrids are shown to be critical for achieving the phase transformation of MoS_2 from the semiconductive 2H to metallic distorted 1T (D-1T) phase.[16] The SA Co-D 1T MoS_2 catalyst exhibits unprecedented Pt-like electrocatalytic activity for HER in acid electrolyte with a very low overpotential of 42 mV at 10 mA cm^{-2}, low Tafel slope of 32 mV dec^{-1} and excellent long-term and cycling stability. The HER activity of SA Co-D 1T MoS_2 is much better than those of any non-noble-metal catalyst reported to date, and very close to that of commercial Pt.[17] The ultrahigh activity is proved to be the ensemble effect through the synergy of single Co atom and S in distorted 1T phase of MoS_2 that possesses the optimal hydrogen binding energy.

Fig. 1a shows the schematic illustration of the preparation of the SA Co-D 1T MoS_2 catalysts using an assembly/leaching process, which ensures the successful introduction of Co atoms on the basal plane other than on the defect or edged sites of MoS_2. Ordered Co NDs with an average diameter of 12 nm and height of 4.5 nm (Supplementary Fig. 1) were first assembled onto the surface of MoS_2 nanosheets by sonication-induced Co-S bonding, in which the assembling amount is highly dependent on the sonication power (Supplementary Fig. 2). Phonons at ultrasonic power may help to closely contact Co nanodisks with MoS_2 nanosheets, and provide the energy for the Co-S bond formation through ultrasonic cavitation (Supplementary Fig. 3-4, Supplementary Table 1).[18,19] The Co ND-modified MoS_2 heterostructures (Co NDs/MoS_2) were further treated by electrochemical CV cycles (Supplementary Fig. 5).[20] This electrochemical CV leaching resulted in the disappearance of Co-Co bond and remaining of Co-S bond in the resultant SA Co-D 1T MoS_2 (Supplementary Fig. 6-7 and Supplementary Table 2). Single-atom Co array was formed and *in-situ* anchored onto the MoS_2 surface, where the Co NDs were assembled. Transmission electron microscopy (TEM) image, selected area electron diffraction (SAED) pattern (Supplementary Fig. 8) and X-ray diffraction (XRD) pattern (Supplementary Fig. 9) show that the Co nanodisks is well contacted with the MoS_2 by forming heterostructures, and there is no Co nanocrystal after the electrochemical leaching. Energy-dispersive X-ray spectroscopy (EDS) mapping analysis reveals that Co is evenly dispersed in SA Co-D 1T MoS_2 (Supplementary Fig. 8f-8h). High-resolution TEM (HRTEM) image shows that MoS_2 is intensely disordered after bonding with Co atoms (Supplementary Fig. 8i). High-angle annular dark-field scanning transmission electron microscopy (HAADF-STEM) was further used to intuitively observe the atomic dispersion of Co and the phase transition of MoS_2 (Fig. 1b-1e). The disordered structure of SA Co-D 1T MoS_2 is totally different from the Moiré patterns when two or few layers of MoS_2 aggregate with random orientation (Supplementary Fig. 10). The atomically isolated Co species (bright spots marked by the red arrow) are dispersed on the D-1T MoS_2 matrix, and the obvious interface between SA Co-D 1T MoS_2 and the 2H MoS_2 is confirmed by both the HAADF-STEM image (Fig. 1c) and simulated pattern (Fig. 1d and 1e). Atomically (electron energy loss spectroscopy) EELS line scanning was also conducted (*inset* of Fig. 1b), showing two Co peaks at 779 eV and 794 eV, which correspond to Co L3 and Co L2, respectively.[21] The statistics for the size of bright dots (Co atom) were determined to be in the range of approximately 2-3 Å, close to

that of a single Co atom (Supplementary Fig. 11).[22] These results indicate that single Co atoms are uniformly bound to the top of the Mo atoms on the MoS_2 slab (Supplementary Fig. 12).[23] The Co mass loading amount on SA Co-D 1T MoS_2 is determined to be 3.54 wt.% by inductively coupled plasma mass spectrometry technique, being in agreement with those determined by EDX technique (3.60 wt.%, Supplementary Fig. 13) and XAFS spectrum simulation (4.07 wt.%, Supplementary Fig. 14). In addition, using the same assembly/leaching strategy, we also successfully prepared SA Ni D-1T MoS_2 and SA Fe D-1T MoS_2 catalysts (Supplementary Fig. 15-25, Supplementary Table 3-4) on the premise that the Ni and Fe nanoplates were used to ensure their large area sufficient contact with MoS_2 instead of their nanoparticles counterparts, further indicating that the method is universal and can be extended to any 2D metals or metal oxides, which meets the criterions.

To verify the coordination environment of atomic Co dispersed on SA Co-D 1T MoS_2, the extended X-ray absorption fine structure (EXAFS) and X-ray absorption near-edge structure (XANES) spectroscopies were performed (Fig. 1f-1g).[24] A single strong shell at 1.79 Å in R-space of the EXAFS spectrum indicates the exclusive existence of Co-S bond for SA Co-D 1T MoS_2 (Fig. 1f).[25,26] The charge density difference from the first principle calculation also confirms the existence of the Co-S covalent bond (Supplementary Fig. 26).[27] We also characterized the cross-section structure and interactions for the side view of the heterostructures. Supplementary Fig. 27 shows the TEM and HAADF-STEM images of the Co NDs-MoS_2. The crystal alignment between Co nanodisks and MoS_2 nanosheets is that the contact layer of Co was covalently bonded with the S atom on the surface of MoS_2, and also the contact layer of MoS_2 nearest to Co nanodisks shows a phase transformation from 2H to distorted 1T phase. We can also observe from the cross-section views of Co nanodisks-MoS_2 that there is a well-defined covalently bounded interface between the counterparts. Using the SA Co-D 1T MoS_2 (Co atom was coordinated with three adjacent sulfur atoms, and located at the site directly above the centre Mo atom) as a model, we also simulated it's XANES spectrum (dotted lines in Fig. 1g).[28] The fitting results for SA Co-D 1T MoS_2 with a Co concentration of 3.70 % show the same two main energy features at 7710 eV (pre-edge) and 7718 eV (white line) as those of the experimental results, further proving that the Co atom is right on the top of Mo atom instead of the replacement of Mo atom. All these extensive experimental and simulation

results reveal that, in SA Co-D 1T MoS_2, a single Co atom is coordinated to three adjacent sulfur atoms and located at the site directly above the Mo atom.

Raman spectra of Co ND/MoS_2 and SA Co-D 1T MoS_2 show peak shifts of E^1_{2g} and A_{1g}, and new peaks between 100 to 350 cm^{-1} (*i.e.*, 126, 149, 195, 214, 236, 283 and 336 cm^{-1}) compared to those of pristine MoS_2 (Fig. 2a), resulting from the phase transformation of the MoS_2.[29] The results from time-dependent evolution of Raman spectra reveal that the phase transformation happened during the assembly process of Co NDs on MoS_2 (Supplementary Fig. 28). The Mo L_3-edge XANES spectrum (Fig. 2b) of SA Co-D 1T MoS_2 shows a decreased peak intensity and blue shift to ~2525.12 eV, indicating the phase transformation from 2H to D-1T MoS_2.[30] The Mo K-edge XANES spectrum (Fig. 2c) of SA Co-D 1T MoS_2 also indicates a considerably widened energy-state distribution related to the Mo 4d electrons with the appearance of some unoccupied Mo 4d states after bonding with the SA Co (as labeled by the arrows).[31] Fig. 2d shows that the second shell intensity of Mo K-edge EXAFS spectrum decreases after the Co NDs assembly. When SA Co-D 1T MoS_2 was produced after CV leaching, the second shell intensity decreases more, indicating the further phase transformation from pristine 2H to D 1T of MoS_2.[32]

The two polymorphs of MoS_2 (pristine 2H phase and distorted 1T phase) can be identified by the XPS spectra of Mo 3d and S 2p. The binding energies of Mo 3d for the pristine 2H MoS_2 (Fig. 2e) are obviously different from those of SA Co-D 1T MoS_2 (Fig. 2f). The peaks at approximately 229.1 and 232.3 eV, corresponding to the binding energies of Mo^{4+} $3d_{5/2}$ and $3d_{3/2}$, shift to lower energy by 0.4 and 0.3 eV, respectively, and also a new doublet of Mo 3d spectrum located at 228.5 and 231.5 eV appears, which indicate the production of distorted 1T MoS_2. The S 2p spectrum also shows a new doublet at 161.6 and 162.7 eV (Supplementary Fig. 29). These new doublets in Mo 3d and S 2p spectra can be assigned to the characteristic peaks of distorted 1T phase MoS_2,[29] further confirming the phase transformation from the pristine 2H to D 1T.[33] The evolution of Co 2P spectrum during the assembly and CV leaching process also confirms the formation of the Co-S bond (Supplementary Fig. 30).

Density functional theory (DFT) calculations were conducted to reveal the mechanism of the phase transition of MoS_2 after assembling Co NDs. On the basal plane of MoS_2 surface, it is found

that there is strong interaction between the Co adatom and S atom. As shown in Fig. 2g, the Co atom prefers to occupy the top site of 2H MoS_2. The adsorption energy is 3.96 eV/Co by the formula, $\Delta E_{ad} = E_{MS} + E_{Co} - E_{MS\text{-}Co}$, where E_{MS}, E_{Co} and $E_{MS\text{-}Co}$, are the energies of the isolated MoS_2, isolated Co atom and MoS_2 with adsorbed Co atom, respectively. Interestingly, the adsorption energy (4.37eV/Co) of Co on 1T MoS_2 (Fig. 2h) is larger than that on 2H MoS_2. This means that Co atoms prefer to bond on 1T MoS_2 than 2H MoS_2. With the adsorption of Co atoms, the energy difference between 2H and 1T ($\mathbf{\Delta E = E_{MS(1T)} - E_{MS(2H)}}$) is 184 meV/atom. That is, the phase transformation of MoS_2 from 2H to 1T is still not thermodynamically favorable, but should be driven by the external force. According to the previous theoretical work, the strain can be used to modulate the phase transition from 2H phase to 1T.[34] In Fig. 2i, the stability of 2H and 1T phases varies with the coverage of Co or the Co-Co distance in the nearest neighbor. Only under the Co-Co distance lesser than 3.10 Å with a strain of about 3.70%, the 1T phase becomes to be more stable (Fig. 2i). It is noticed that the Co-Co distance on (111) facet of Co is about 2.51 Å and the lattice constant of MoS_2 is about 3.16 Å. The mismatch between the lattice of metallic Co and pristine 2H MoS_2 is large enough for the strain generation (Supplementary Fig. 31). In this case, the anchoring of Co atoms induces the coordination reconstruction of the MoS_2 support to D-1T MoS_2 due to a charge-density wave (CDW) state.[35] Such CDW state of D-1T MoS_2 can trap the system into the deeper energy minimum on the potential energy surface. The CDW structures with different Co coverages are illustrated in Supplementary Fig. 32. These DFT results strongly support the experimental observation that phase transition happens after the assembly of Co NDs on MoS_2 surface, during which the Co-S bond was formed with the assistance of sonication.

The HER activities of the catalysts were studied in 0.5 M H_2SO_4 solution. SA Co-D 1T MoS_2 with 3.54% Co loading amount exhibits an extremely small onset overpotential (η) of 42 mV *vs.* the reversible hydrogen electrode (RHE) for HER, much smaller than those of other non-precious metal catalysts and even comparable to that of 10% Pt/C (Fig. 3a, Supplementary Fig. 33, Supplementary Table 5-6). To gain a quantitative insight into the HER activity, the turnover frequency (TOF), which can reveal the intrinsic catalytic activity of a single active site of the catalyst, was calculated (Supplementary Fig. 34). SA Co-D 1T MoS_2 shows a TOF of 7.82 s^{-1} at an overpotential of 100 mV

179 *vs.* RHE, the highest value among all previously reported non-Pt catalysts to date.[36] Also, after the
180 SA Co atom bonding, the catalyst shows a lower EIS response than the MoS_2 (Supplementary Fig.
181 35), indicating a fast kinetics for hydrogen evolution.[37] The Tafel slope of SA Co-D 1T MoS_2 is 32
182 mV dec^{-1} (Fig. 3b), similar to that of Pt/C (30 mV dec^{-1}), and surpassing those of previously reported
183 non-Pt-based materials (Fig. 3c) that using a graphite rod as the counter electrode instead of Pt foil to
184 avoid Pt contamination.[38] The low Tafel slope indicates that SA Co-D 1T MoS_2 processes a Tafel
185 rate-determining-step mechanism for HER, instead of the common Volmer reaction.[39] In addition, a
186 series of control experiments and DFT calculations prove that other MoS_2/Co catalysts prepared by
187 using Co clusters, nanoparticles, or ions on MoS_2 cannot achieve such high HER performance
188 (Supplementary Fig. 36-45, Supplementary Table 7). The SA Ni D-1T MoS_2 and SA Fe D-1T MoS_2
189 catalysts also show enhanced HER activity relative to pristine MoS_2, but lower than SA Co D-1T
190 MoS_2 (Supplementary Fig. 46 and Supplementary Table 8).

191 SA Co-D 1T MoS_2 shows excellent cycling stability and long-term durability for HER in acidic
192 media. The linear sweep voltammetry (LSV) curves measured for SA Co-D 1T MoS_2 before and
193 after 10,000 CV cycles between 0.1 and -0.3 V *vs.* RHE exhibit a negligible current density loss (Fig.
194 3d). Fig. 3e shows the long-term durability measured by performing continuous HER at a static
195 overpotential of 100 mV. Consistent H_2 generation was observed during the HER process (*inset* of
196 Fig. 3e), and the current density remained without any decrease as the reaction proceeded for 10 days.
197 The high stability of SA Co-D 1T MoS_2 catalyst was also confirmed by HAADF-STEM (atomic
198 structure stability), XPS (valence state and phase stability), XANES and FT-EXAFS (coordination
199 environment stability) after accelerating stability measurements, long-term air storage and heating
200 treatment (Supplementary Fig. 47-52 and Supplementary Table 9).

201 The nature of the unprecedented activity of SA Co D-1T MoS_2 was disclosed by comparing the
202 HER polarization plots of different catalysts (Fig. 3f). The HER activity of MoS_2 was first improved
203 by the assembly of Co NDs (Step 1, Co NDs/MoS_2) that induced the phase transformation from 2H
204 to D-1T (onset overpotential decreases from 162 mV to 85 mV at 10 mA cm^{-2}) because the metallic
205 1T MoS_2 can give higher conductivity and more active sites for better HER.[40] The HER performance
206 of MoS_2 was further improved to a Pt-like activity (onset overpotential decreases from 85 mV to 42

mV, similar to the Pt/C, by CV leaching to form single atom Co sites on D-1T MoS_2 (Step 2, SA Co D-1T MoS_2). Thiocyanate ion (SCN^-, poisoning agent) was then used to block the Co active sites.[41] The addition of 10 mM SCN^- resulted in an increase of onset overpotential from 42 mV to 112 mV (Step 3, SA Co-D 1T MoS_2 with SCN^-), close to that of the 1T MoS_2 prepared by lithiation. Therefore, the unprecedented HER activity of the SA Co-D 1T MoS_2 catalyst is a synergetic effect of both the single Co atom and the D-1T MoS_2, that is to say, both single Co atom site and 2H to D-1T phase transformation of MoS_2 are contributory. Nevertheless, single atom Co sites give the dominant contribution to Pt-like HER activity.

DFT calculations were further performed to explore the origin of the unprecedented electrocatalytic activity of SA Co-D 1T MoS_2 for the HER in acidic solution. According to the DFT calculations, the PDOS of Co 3d near the Fermi level for 3×3 and 4×4 cases are remarkably different from the others (Fig. 4a). It indicates that the Co adatoms are transformed from cationic to metallic with the coverage increasing to 2.08% and 3.70% (corresponding to 4×4 and 3×3 models) because of their transition CDW structures. In particular, the resulted increase in the empty state of Co close to the Fermi level for the 3×3 case is the most significant among the systems studies, being able to promote the hybridization between Co adatom and the hydrogen atom, and thus enhance the corresponding hydrogen binding. In addition, the d-peak at the Fermi level for the 3×3 case is stronger than that for 4×4 case, indicating the stronger hydrogen adsorption on cobalt. Such variation in Co 3d with the coverage strongly depends on the Co-MoS_2 interaction, which corresponds to the so called electronic or ligand effect. The $|\Delta G_{H*}|$ value is dependent on the Co coverage on D-1T MoS_2 (Fig. 4b). SA Co-D 1T MoS_2 with a Co coverage of 3.70% (3×3 superstructure) shows the lowest $|\Delta G_{H*}|$ value of 0.03 eV, enabling the HER energy profile even closer to the ideal than Pt (111) with the $|\Delta G^{Pt}_{H*}|$ = 0.09 eV. Thus, a superior HER activity of SA Co-D 1T MoS_2 catalyst over Pt is expected from a thermodynamics viewpoint (Supplementary Fig. 53-55).

Most importantly, the prominent HER activity of SA Co-D 1T MoS_2 in a 3×3 superstructure is attributed to the "ensemble effect" of D-1T MoS_2 support and Co single atom. Our calculation results show that the hydrogen adsorption at the upright position of Co on MoS_2 (111) is not as favorable as that at the tilted top site toward the adjacent S atom on the surface (Fig. 4c) by 0.68 eV/unit. The

preference for the tilted top site is associated with the ensemble effect at the Co-MoS_2 (111) interface. The energy gain by moving from the upright to the tilted position is associated with the electrostatic attraction between the positively charged proton and negatively charged S adjacent to Co. Fig. 4e plots the variation in Hirshfeld charge of Co and adjacent S as a function of Co coverage.[44] The positive Co atom is beneficial to the protonation process. Among the S ions, the one in a 3×3 superstructure displays the most negative charge, and therefore contributes the most to stabilize adsorbed H *via* the electrostatic interaction. Our DFT calculations highlight the importance of ensemble effect *via* the synergy of Co adatom and S of the MoS_2 (111) support in tuning hydrogen binding mode at the interface and thus achieving superior HER activity.

In summary, we report a newly designed single-atom array catalyst, SA Co-D 1T MoS_2, with Pt-like HER performance by a new top-down assembly/leaching strategy. During the assembly process, the strain induced by lattice mismatch and the formation of the covalent Co-S bond between Co ND and 2H MoS_2 nanosheet are identified as the main reasons for 2H to D 1T phase transformation. The 2D morphology of Co NDs is the key in the preparation of SA Co-D IT MoS_2 because that the large area contact of Co with the basal plane of MoS_2 is essential to generate enough compressive strain for phase transformation. The active-site blocking experiment reveals that the single-atom Co in SA Co-D 1T MoS_2 is the principal catalytic centre, although both single Co atom and 2H to D-1T phase transformation of MoS_2 are contributory for HER catalysis. DFT calculations confirm that the unprecedented HER activity of this single atom catalyst is mainly due to an ensemble effect *via* the synergy of Co adatom and S of the MoS_2 (111) support by tuning hydrogen binding mode at the interface. The discovery of this SA Co-D 1T MoS_2 catalyst highlights a new area of tuning the structure and functionality of metal-TMD catalysts at the atomic scale, which holds promise for applications in large-scale water splitting electrolysers.

Acknowledgement

This work was financially supported by the National Key R&D Program of China (2016YFA0200400 and 2017YFA0206701), the National Natural Science Foundation of China (51571100, 21275064 and 51671003), and Program for JLU Science and Technology Innovative Research Team (JLUSTIRT, 2017TD-09), the Specialized Research Fund for the Doctoral Program

of Higher Education (20130061110035) and start-up supports from Peking University and the Young Thousand Talented Program. Part of DFT studies were performed at Brookhaven National Laboratory supported by the U.S. Department of Energy (DOE), Office of Science, Office of Basic Energy Sciences, Division of Chemical Sciences, Biosciences and Geosciences, under contract No. DE-SC0012704. We thank the Beijing Synchrotron Radiation Facility (BSRF) for providing beam time on beamline 1W1B for the XAS measurements. We thank the Shanghai Synchrotron Radiation Facility (SSRF) for providing beam time on beamline BL14W1 for the XAS measurements. We express our sincere thanks to Peng Zhang, Wei Du and Zhiliang Cheng for their discussions and help.

Supplementary Information accompanies the paper on **www.nature.com/nature.**

Materials and Methods, Supplementary Fig. 1-55, Supplementary Table 1-9, and References 1-67.

References

1 Voiry, D. *et al.* Low dimensional catalysts for hydrogen evolution and CO_2 reduction. *Nat. Rev. Chem.* **1**, 0105 (2018).

2 Cabán-Acevedo, M. *et al.* Efficient hydrogen evolution catalysis using ternary pyrite type cobalt phosphosulphide. *Nat. Mater.* **14**, 1245-1251 (2015).

3 Seh, Z. W. *et al.* Combining theory and experiment in electrocatalysis: Insights into materials design. *Science* **355**, eaad4998 (2017).

4 Li, Y. G. *et al.* MoS_2 nanoparticles grown on graphene: An advanced catalyst for the hydrogen evolution reaction. *J. Am. Chem. Soc.* **133**, 7296-7299 (2011).

5 Zou, X. X. *et al.* Noble metal-free hydrogen evolution catalysts for water splitting. *Chem. Soc. Rev.* **44**, 5148-5180 (2015).

6 Jaramillo, T. F. *et al.* Identification of active edge sites for electrochemical H_2 evolution from MoS_2 nanocatalysts. *Science* **317**, 100-102 (2007).

7 Li, H. *et al.* Activating and optimizing MoS_2 basal planes for hydrogen evolution through the formation of strained sulphur vacancies. *Nat. Mater.* **15**, 48-53 (2015).

8 Liu, P. *et al.* Photochemical route for synthesizing atomically dispersed palladium catalysts. *Science* **352**, 797-800 (2016).

9 Xue, Y. *et al.* Anchoring zero valence single atoms of nickel and iron on graphdiyne for hydrogen evolution. *Nat. Commun.* **9**, 1460 (2018).

10 Li, H. *et al.* Synergetic interaction between neighbouring platinum monomers in CO_2 hydrogenation. *Nat. Nanotechnol.* **13**, 411-417 (2018).

11 Xu, H. *et al.* A universal principle for a rational design of single-atom electrocatalysts. *Nat. Catal.* **1**, 339-348 (2018).

12 Wang, A. *et al.* Heterogeneous single atom catalysis. *Nat. Rev. Chem.* **2**, 65-81 (2018).

13 Zhu, C. *et al.* Single atom electrocatalysts. *Angew. Chem. Int. Ed.* **56**, 13944-13960 (2017).

14 Voiry, D. *et al.* The role of electronic coupling between substrate and 2D MoS_2 nanosheets in electrocatalytic production of hydrogen. *Nat. Mater.* **15**, 1003-1009 (2016).

15 O'Connor, N. J. *et al.* Interaction trends between single metal atoms and oxide supports identified with density functional theory and statistical learning. *Nat. Catal.* **1**, 531-539 (2018).

16 Lin, Y.-C. *et al.* Atomic mechanism of the semiconducting to metallic phase transition in single layered MoS_2. *Nat. Nanotechnol.* **9**, 391-396 (2014).

17 Staszak-Jirkovský, J. *et al.* Design of active and stable Co-Mo-S_x chalcogels as pH-universal catalysts for the hydrogen evolution reaction. *Nat. Mater.* **15**, 197-203 (2016).

18 Black, C. *et al.* Spin dependent tunneling in self assembled cobalt nanocrystal superlattices. *Science* **290**, 1131-1134 (2000).

19 Shi, X. Y. *et al.* Metallic contact between MoS_2 and Ni via Au nanoglue. *Small* **14**, 1704526 (2018).

20 Fan, L. *et al.* Atomically isolated nickel species anchored on graphitized carbon for efficient hydrogen evolution electrocatalysis. *Nat. Commun.* **7**, 10667 (2016).

21 Li, C. S. *et al.* High performance hybrid oxide catalyst of manganese and cobalt for low pressure methanol synthesis. *Nat. Commun.* **6**, 6538 (2015).

22 Yang, L. *et al.* Single atom cobalt electrocatalysts for foldable solid state Zn-air battery. *Nano Energy* **50**, 691-698 (2018).

23 Liu, G. *et al.* MoS_2 monolayer catalyst doped with isolated Co atoms for the

hydrodeoxygenation reaction. *Nat. Chem.* **9**, 810-816 (2017).

24 Koziej, D. Revealing complexity of nanoparticle synthesis in solution by *in-situ* hard X-ray spectroscopy-Today and beyond. *Chem. Mater.*, 2478-2490 (2016).

25 Kornienko, N. *et al. Operando* spectroscopic analysis of an amorphous cobalt sulfide hydrogen evolution electrocatalyst. *J. Am. Chem. Soc.* **137**, 7448-7455 (2015).

26 Pan, Y. *et al.* Design of single atom Co-N_5 catalytic site: A robust electrocatalyst for CO_2 reduction with nearly 100% CO selectivity and remarkable stability. *J. Am. Chem. Soc.* **140**, 4218-4221 (2018).

27 Kasai, H. *et al.* X-ray electron density investigation of chemical bonding in van der Waals materials. *Nat. Mater.* **17**, 249-252 (2018).

28 Liu, W. *et al.* Single atom dispersed Co-N-C catalyst: structure identification and performance for hydrogenative coupling of nitroarenes. *Chem. Sci.* **7**, 5758-5764 (2016).

29 Yu, Y. *et al.* High phase purity 1T'-MoS_2 and 1T'-$MoSe_2$ layered crystals. *Nat. Chem.* **10**, 638-643 (2018).

30 Cai, L. *et al.* Vacancy induced ferromagnetism of MoS_2 nanosheets. *J. Am. Chem. Soc.* **137**, 2622-2627 (2015).

31 Deng, J. *et al.* Multiscale structural and electronic control of molybdenum disulfide foam for highly efficient hydrogen production. *Nat. Commun.* **8**, 14430 (2017).

32 Zhao, X. *et al.* FeS_2 doped MoS_2 nanoflower with the dominant 1T MoS_2 phase as an excellent electrocatalyst for high performance hydrogen evolution. *Electrochim. Acta* **249**, 72-78 (2017).

33 Tan, C. *et al.* Preparation of single layer $MoS_{2x}Se_{2(1-x)}$ and $Mo_xW_{1-x}S_2$ nanosheets with high concentration metallic 1T phase. *Small* **12**, 1866-1874 (2016).

34 Song, S. *et al.* Room temperature semiconductor metal transition of $MoTe_2$ thin films engineered by strain. *Nano Lett.* **16**, 188-193 (2015).

35 Whangbo, M. H. *et al.* Analogies between the concepts of molecular chemistry and solid-state physics concerning structural instabilities. Electronic origin of the structural modulations in layered transition metal dichalcogenides. *J. Am. Chem. Soc.* **114**, 9587-9600 (1992).

36 Kibsgaard, J. *et al.* Building an appropriate active site motif into a hydrogen evolution

catalyst with thiomolybdate $[Mo_3S_{13}]^{2-}$ clusters. *Nat. Chem.* **6**, 248-253 (2014).

37 Zhang, X. W. *et al.* Amorphous MoS_xCl_y electrocatalyst supported by vertical graphene for efficient electrochemical and photoelectrochemical hydrogen generation. *Energ. Environ. Sci.* **8**, 862-868 (2015).

38 Chen, R. *et al.* Use of platinum as the counter electrode to study the activity of nonprecious metal catalysts for the hydrogen evolution reaction. *ACS Energy Lett.* **2**, 1070-1075 (2017).

39 Liang, H. *et al.* Molecular metal-N_x centres in porous carbon for electrocatalytic hydrogen evolution. *Nat. Commun.* **6**, 7992 (2015).

40 Geng, X. *et al.* Pure and stable metallic phase molybdenum disulfide nanosheets for hydrogen evolution reaction. *Nat. Commun.* **7**, 10672 (2016).

41 Wang, Q. *et al.* Phenylenediamine based FeN_x/C catalyst with high activity for oxygen reduction in acid medium and its active site probing. *J. Am. Chem. Soc.* **136**, 10882-10885 (2014).

42 Nørskov, J. K. *et al.* Towards the computational design of solid catalysts. *Nat. Chem.* **1**, 37-46 (2009).

43 Seh, Z. W. *et al.* Combining theory and experiment in electrocatalysis: Insights into materials design. *Science* **355**, eaad4998 (2017).

44 Hirshfeld, F. L. Bonded-atom fragments for describing molecular charge densities. *Theor. Chim. Acta B* **44**, 129-138 (1977).

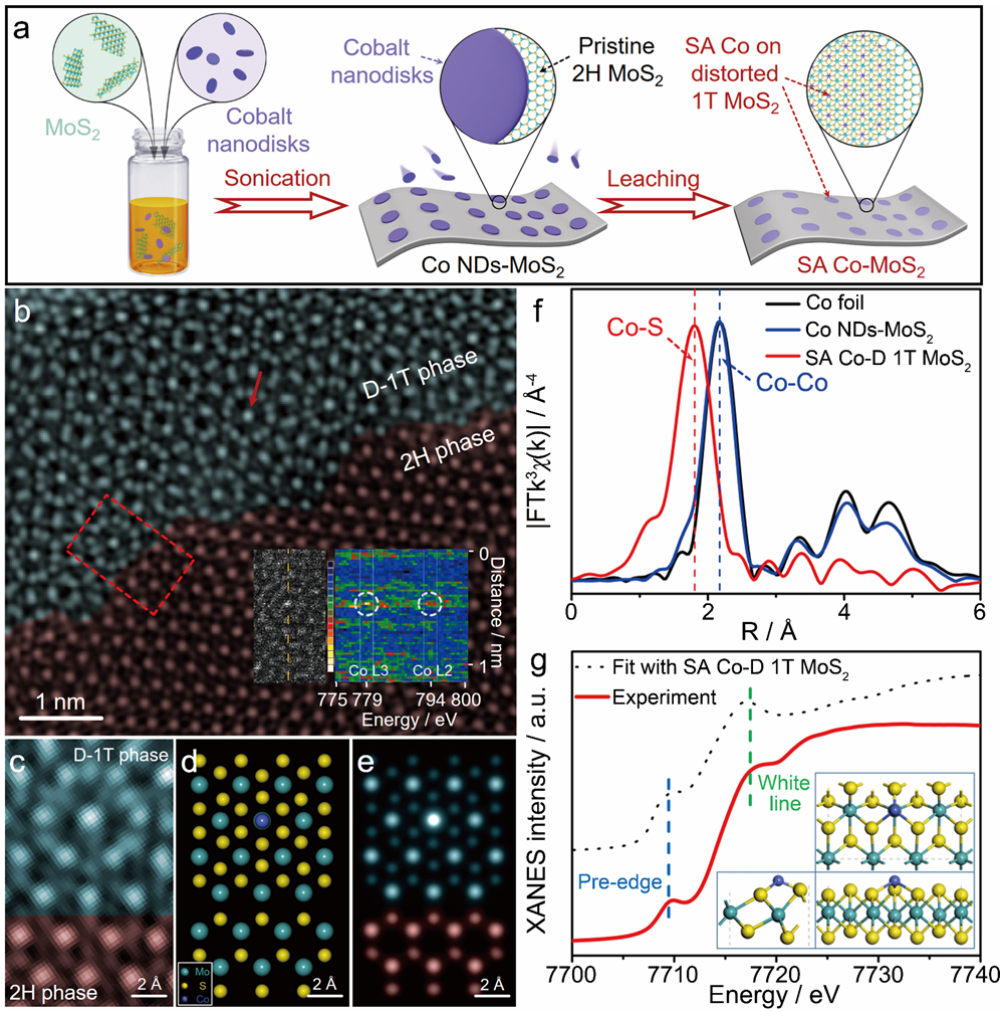

Figure 1 | Schematic illustration of synthetic method for SA Co-D 1T MoS_2 and its characterization. **a**, Schematic diagram of the fabrication process for SA Co-D 1T MoS_2. **b**, Aberration-corrected HAADF-STEM image of SA Co-D 1T MoS_2, showing the obvious junction between SA Co-D 1T MoS_2 (dark cyan) and pristine 2H MoS_2 (wine). The *inset* shows the HRTEM and EELS spectrum of SA Co-D 1T MoS_2. **c**, Enlarged HAADF-STEM image in the red square area of b. **d**, Theoretical model and **e**, simulated STEM images using QSTEM simulation software. **f**, FT-EXAFS spectra of SA Co-D 1T MoS_2 and bulk cobalt foil at the Co K-edge. **g**, Co K-edge XANES of SA Co-D 1T MoS_2 and fitted curve. The *inset* shows the atomic structure of SA Co-D 1T MoS_2.

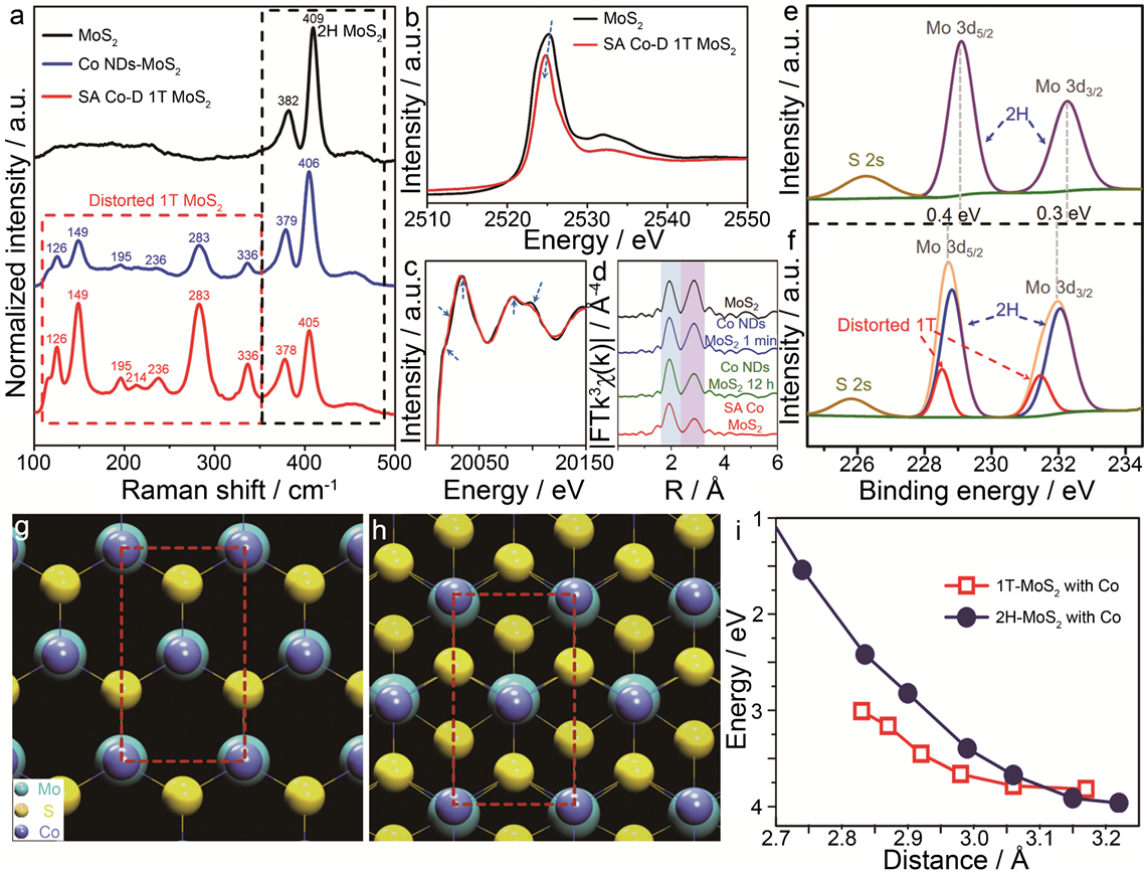

Figure 2 | Characterization techniques and DFT calculation for the phase transformation of MoS_2. a, Raman spectra of pristine MoS_2, Co NDs/MoS_2 and SA Co-D 1T MoS_2. **b-c**, Mo L_3-edge and K-edge XANES spectra of SA Co-D 1T MoS_2 and pristine MoS_2. d, Mo K-edge EXAFS spectra variation during the preparation of SA Co-D 1T MoS_2. **e-f**, Mo 3d XPS spectra show the surface binding state variation before **e** and **f** after the MoS_2 phase transformation. **g**, 2H and **h**, 1T atomic structures of MoS_2 assembled with Co atomic layer calculated by first-principles. **i**, Energies of 2H MoS_2 and 1T MoS_2 assembled with Co atomic layer as a function of Co-Co distance calculated by first principles method based on the single layer 2H MoS_2 and atomic Co as the reference state with the formula $\Delta E = E_{2H\text{-}MS} + E_{Co} - E_{MS\text{-}Co}$.

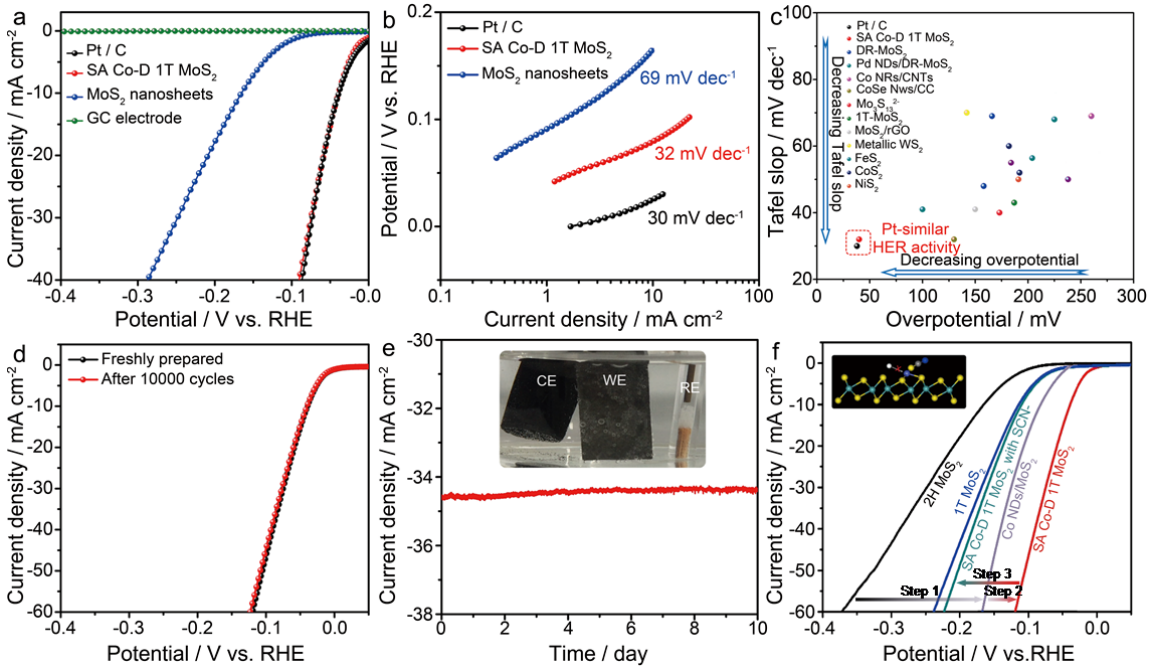

Figure 3 | HER performance of SA Co-D 1T MoS_2. a, Polarization curves of different catalysts tested in Ar-saturated 0.5 M H_2SO_4. **b**, Tafel plots for the catalysts derived from **a**. **c**, HER activity comparison using the Tafel slope (mV dec^{-1}) *vs.* overpotential at a current density of 10 mA cm^{-2}. **d**, Polarization curves of the SA Co-D 1T MoS_2 after 10,000 CV cycles. **e**, Time dependence of the current density for SA Co-D 1T MoS_2 at a static overpotential of 100 mV *vs.* RHE. **f**, HER polarization plots of MoS_2, 1T MoS_2 prepared by lithiation, Co NDs/MoS_2 and SA Co-D 1T MoS_2 without and with SCN^- ions. The *inset* shows that the cobalt HER active centres are blocked by SCN^- ions.

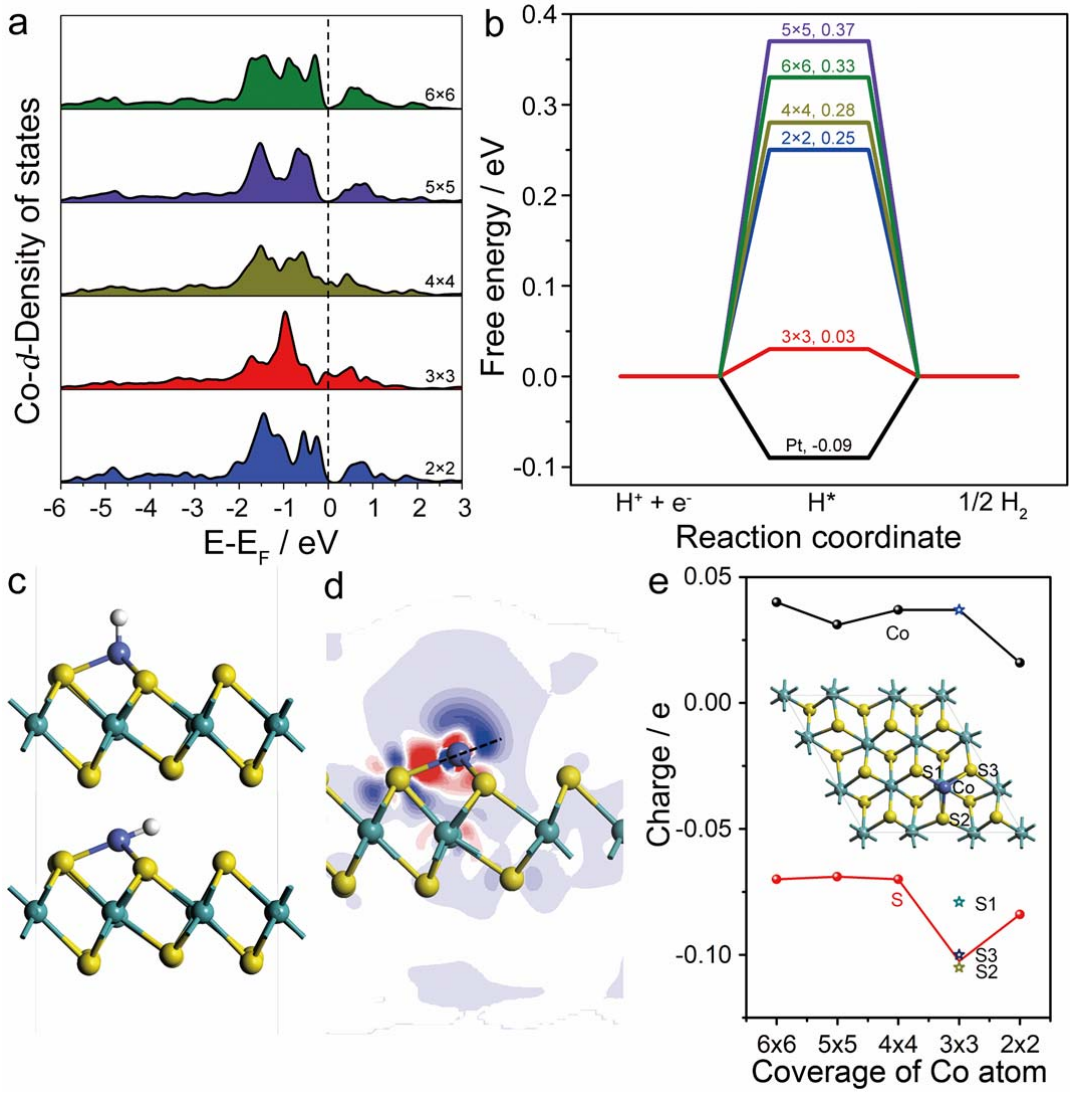

Figure 4 | Theoretical calculation of SA Co-D 1T MoS_2 for HER. a, Calculated Co projected d-density of states for different coverage. **b**, Calculated free-energy diagram for HER at a potential of U = 0 relative to the standard hydrogen electrode at pH = 0 for different atomic Co loading amounts. **c,** Hydrogen adsorption modes on the single atom Co-MoS_2 3x3 case. **d**, The electron density difference of 3x3 case and **e**, The electron charge of Co and S adjacent to Co as a function of Co coverage.